

Luminescent One- And Two-Dimensional Extended Structures and a Loosely Associated Dimer Based on Platinum(II)–Thallium(I) Backbones[†]

Juan Forniés,^{*,‡} Ana García,[§] Elena Lalinde,^{*,§} and M. Teresa Moreno[§]

Departamento de Química Inorgánica, Instituto de Ciencia de Materiales de Aragón, Universidad de Zaragoza-Consejo Superior de Investigaciones Científicas, 50009 Zaragoza, Spain, and Departamento de Química-Grupo de Síntesis Química de La Rioja, UA-CSIC, Universidad de La Rioja, 26006 Logroño, Spain.

Received November 6, 2007

Neutralization reactions between $(\text{NBu}_4)_2[\text{trans-Pt}(\text{C}_6\text{F}_5)_2(\text{CN})_2]$ **1** and $(\text{NBu}_4)_2[\text{cis-Pt}(\text{C}_6\text{F}_5)_2(\text{CN})_2]$ **2** with TIPF_6 have been carried out, and the resulting structures of $[\text{trans,trans,trans-Tl}_2\{\text{Pt}(\text{C}_6\text{F}_5)_2(\text{CN})_2\} \cdot (\text{CH}_3\text{COCH}_3)_2]_n$ **[4 · (CH₃COCH₃)₂]_n** and $\{\text{Tl}\{\text{Ti}\{\text{cis-Pt}(\text{C}_6\text{F}_5)_2(\text{CN})_2\}\} \cdot (\text{H}_2\text{O})\}_n$ **[5 · (H₂O)]_n** have been determined by X-ray crystallography. Remarkably, the change from *trans* to *cis* geometry on the platinum substrate causes a significant decrease in the $\text{Pt}^{\text{II}} \cdots \text{Tl}^{\text{I}}$ metallophilic interaction. Thus, the platinum center in the *trans* fragment easily connects with two Tl^I ions forming a distorted pseudo-octahedron PtTl_2 , which generates a final two-dimensional layered structure by secondary additional intermolecular $\text{Tl}^{\text{I}} \cdots \text{N}(\text{CN})$ interactions. However, the $[\text{cis-Pt}(\text{C}_6\text{F}_5)_2(\text{CN})_2]^{2-}$ fragment interacts strongly with just one Tl center leading to an extended helical $[-\text{Pt}-\text{Tl}-\text{Pt}-\text{Tl}-]_n^{n-}$ chain. In this case, the second thallium center neutralizes the anionic chain mainly through $\text{Tl}^{\text{I}} \cdots \text{N}(\text{CN})$ (*intra*) and $\text{Tl}^{\text{I}} \cdots \text{F}(\text{C}_6\text{F}_5)$ (*intra* and *inter*) interactions. The reaction of TIPF_6 with the monoanionic fragment $(\text{NBu}_4)[\text{cis-Pt}(\text{C}_6\text{F}_5)_2(\text{CN})(\text{PPh}_2\text{C}\equiv\text{CPh})]$ **3** yields the discrete associated dimer $[\text{Tl}\{\text{cis-Pt}(\text{C}_6\text{F}_5)_2(\text{CN})(\text{PPh}_2\text{C}\equiv\text{CPh})\}]_2$ **[6]₂**. Dimer **[6]₂** could be described as two square pyramids with the thallium atoms in the apical positions, connected through $\text{Tl}^{\text{I}} \cdots \text{N}(\text{cyano})$ interactions. The final heteropolynuclear Pt–Tl complexes, except **4** at room temperature, show bright emission in the solid state when irradiated with UV–vis radiation, in contrast to the precursors **1** and **3**, which are not luminescent. This difference indicates that the emissions in **4–6** are presumably related to the interaction between the metal centers. The Pt–Tl bonding interactions and, consequently, the emissive properties are lost in solution at room temperature, as shown by the conductivity and NMR measurements. However, variable-concentration luminescence measurements in glassy acetonitrile solutions indicate the formation of different aggregates with different degrees of $\text{Pt} \cdots \text{Tl}$ interactions for **4** and **5** and a dimeric structure similar to that observed in solid state for **6**.

Introduction

Metal–ligand coordination and non covalent intermolecular interactions such as hydrogen bonding, π – π stacking, and^{1–9} electrostatic and van der Waals interactions have been used to generate a wide variety of molecular assemblies in supramolecular chemistry. Polynuclear assemblies based on

weak interactions between closed shell or subclosed shell (d^{10} , s^2 , and d^8) metal centers have also attracted much attention because of their intriguing structural diversity and interesting photoluminescent behavior with potential applications.^{10–22} In this area, the presence of direct platinum–

[†] Dedicated to Professor Gregorio Asensio, Universidad de Valencia, on the occasion of his 60th anniversary.

* To whom correspondence should be addressed. E-mail: juan.fornies@unizar.es (J.F.), elena.lalinde@unirioja.es (E.L.).

[‡] Universidad de Zaragoza.

[§] Universidad de La Rioja.

(1) Lehn, J. M. *Supramolecular Chemistry: Concepts and Perspectives*; VCH: Weinheim, Germany, 1995.

(2) Haiduc, I.; Edelman, F. T. *Supramolecular Organometallic Chemistry*; Wiley-VCH: Weinheim, Germany, 1999.

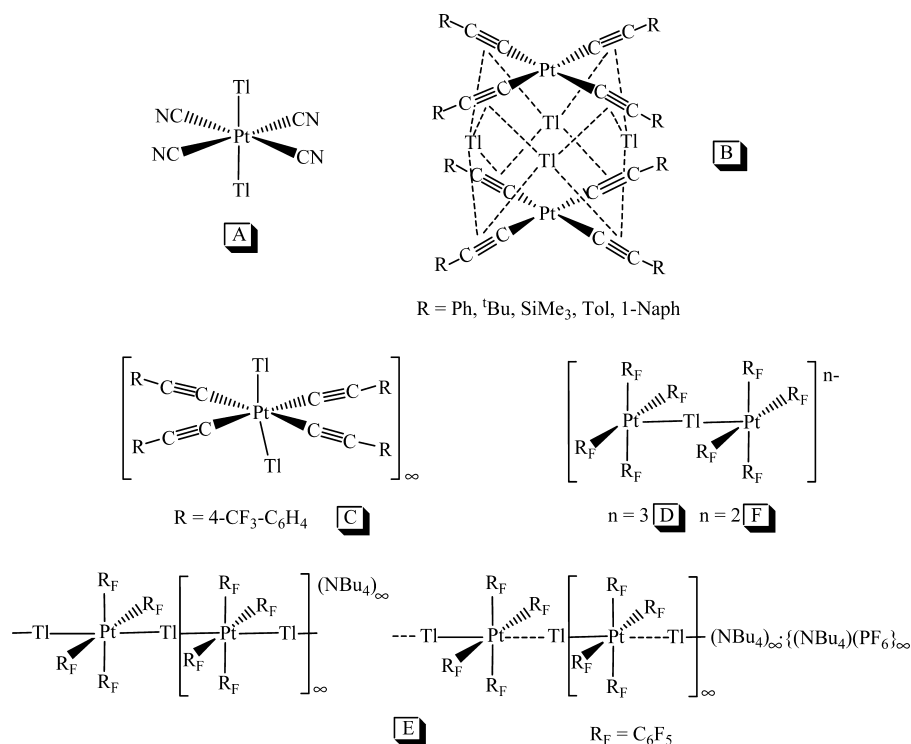
(3) Tiekink, E. R. T.; Vittal, J. J. *Frontiers in Crystal Engineering*; Wiley: Chichester, 2006.

(4) Omary, M. A.; Mohamed, A. A.; Rawashdeh-Omary, M. A.; Fackler, J. P., Jr. *Coord. Chem. Rev.* **2005**, *249*, 1372.

(5) Oh, M.; Carpenter, G. B.; Sweigart, D. A. *Acc. Chem. Res.* **2004**, *37*, 1.

(6) Roesky, H. W.; Adruh, M. *Coord. Chem. Rev.* **2003**, *236*, 91.

Chart 1



thallium bonds is often associated with intense photoluminescence.^{23–35} The first report dates back to 1988 when Balch and co-workers examined the luminescence behavior of

crystals of [PtTl₂(CN)₄]³⁵ (A, Chart 1) (λ_{em} 444 nm, 298 K). Later works have shown that emission bands cover a wide range (444–700 nm), depending on the compound. Platinum–thallium polynuclear complexes are also interesting because of their structural and other spectroscopic (¹⁹⁵Pt NMR) properties.^{23,34,36–46} Four types of bonding situations have been observed, depending on the formal oxidation state of metal centers: (Pt⁰–Tl^I),^{10,38–40,47–49} (Pt^{II}–Tl^I),^{23–27,29,30,34,35,37,50–57}

- (7) Sun, S. S.; Lees, A. J. *Coord. Chem. Rev.* **2002**, *230*, 170–191.
- (8) Khlobystov, A. N.; Blake, A. J.; Champness, N. R.; Lemenovskii, D. A.; Majouga, A. G.; Zyk, N. V.; Schröder, M. *Coord. Chem. Rev.* **2001**, *222*, 155.
- (9) Fujita, M. *Chem. Soc. Rev.* **1998**, *27*, 417.
- (10) Gade, L. H. *Angew. Chem., Int. Ed.* **2001**, *40*, 3573.
- (11) Pyykkö, P. *Chem. Rev.* **1997**, *97*, 597.
- (12) Pyykkö, P. *Angew. Chem., Int. Ed.* **2004**, *43*, 4412.
- (13) Fung, E. Y.; Olmstead, M. M.; Vickery, J. C.; Balch, A. L. *Coord. Chem. Rev.* **1998**, *171*, 151.
- (14) Fernández, E. J.; Laguna, A.; López de Luzuriaga, J. M. *Coord. Chem. Rev.* **2005**, *249*, 1423.
- (15) Williams, J. M.; Schultz, A. J.; Underhill, A. E.; Carneiro, K. In *Extended Linear Chain Compounds*; Miller, J. S., Ed.; Plenum Press: New York, 1982.
- (16) Bera, J. K.; Dunbar, K. R. *Angew. Chem., Int. Ed.* **2002**, *41*, 4453.
- (17) Che, C. M.; Lai, S. W. *Coord. Chem. Rev.* **2005**, *249*, 1296.
- (18) Evans, R. C.; Douglas, P.; Winscom, C. J. *Coord. Chem. Rev.* **2006**, *250*, 2093.
- (19) Yam, V. W. W. *Acc. Chem. Res.* **2002**, *35*, 555.
- (20) Puddephatt, R. J. *Coord. Chem. Rev.* **2001**, *216–217*, 313.
- (21) Ford, P. C.; Vogler, A. *Acc. Chem. Res.* **1993**, *26*, 220.
- (22) Yam, V. W. W.; Lo, K. K. W.; Wong, K. M. C. *J. Organomet. Chem.* **1999**, *578*, 3.
- (23) Chen, W.; Liu, F.; Xu, D.; Matsumoto, K.; Kishi, S.; Kato, M. *Inorg. Chem.* **2006**, *45*, 5552.
- (24) Falvello, L. R.; Forniés, J.; Garde, R.; García, A.; Lalinde, E.; Moreno, M. T.; Steiner, A.; Tomás, M.; Usón, I. *Inorg. Chem.* **2006**, *45*, 2543.
- (25) Berenguer, J. R.; Forniés, J.; Gil, B.; Lalinde, E. *Chem.—Eur. J.* **2006**, *12*, 785.
- (26) Charmant, J. P. H.; Forniés, J.; Gómez, J.; Lalinde, E.; Merino, R. I.; Moreno, M. T.; Orpen, A. G. *Organometallics* **2003**, *22*, 652.
- (27) Berenguer, J. R.; Forniés, J.; Gómez, J.; Lalinde, E.; Moreno, M. T. *Organometallics* **2001**, *20*, 4847.
- (28) Jalilievand, F.; Eriksson, L.; Glaser, J.; Maliarik, M.; Mink, J.; Sandström, M.; Tóth, I.; Tóth, J. *Chem.—Eur. J.* **2001**, *7*, 2167.
- (29) Usón, R.; Forniés, J.; Tomás, M.; Garde, R.; Merino, R. I. *Inorg. Chem.* **1997**, *36*, 1383.
- (30) Ara, I.; Berenguer, J. R.; Forniés, J.; Gómez, J.; Lalinde, E.; Merino, R. I. *Inorg. Chem.* **1997**, *36*, 6461.
- (31) Dolg, M.; Pyykkö, P.; Runeberg, N. *Inorg. Chem.* **1996**, *35*, 7450.
- (32) Clodfelter, S. A.; Doede, T. M.; Brennan, B. A.; Nagle, J. K.; Bender, D. P.; Turner, W. A.; LaPunzina, P. M. *J. Am. Chem. Soc.* **1994**, *116*, 11379.
- (33) Weissbart, B.; Balch, A. L.; Tinti, D. S. *Inorg. Chem.* **1993**, *32*, 2096.
- (34) Balch, A. L.; Rowley, S. P. *J. Am. Chem. Soc.* **1990**, *112*, 6139.
- (35) Nagle, J. K.; Balch, A. L.; Olmstead, M. M. *J. Am. Chem. Soc.* **1988**, *110*, 319.
- (36) Chen, W.; Liu, F.; Matsumoto, K.; Autschbach, J.; Le Guennic, B.; Ziegler, T.; Maliarik, M.; Glaser, J. *Inorg. Chem.* **2006**, *45*, 4526.
- (37) Oberbeckmann-Winter, N.; Braunstein, P.; Welter, R. *Organometallics* **2004**, *23*, 6311.
- (38) Catalano, V. J.; Malwitz, M. A. *J. Am. Chem. Soc.* **2004**, *126*, 6560.
- (39) Catalano, V. J.; Bennett, B. L.; Yson, R. L.; Noll, B. C. *J. Am. Chem. Soc.* **2000**, *122*, 10056.
- (40) Catalano, V. J.; Bennett, B. L.; Muratidis, S.; Noll, B. C. *J. Am. Chem. Soc.* **2001**, *123*, 173.
- (41) Ma, G.; Maliarik, M.; Sun, L.; Glaser, J. *Inorg. Chim. Acta* **2004**, *357*, 4073.
- (42) Jalilievand, F.; Maliarik, M.; Sandström, M.; Mink, J.; Persson, I.; Persson, P.; Tóth, I.; Glaser, J. *Inorg. Chem.* **2001**, *40*, 3889.
- (43) Ma, G.; Kritikos, M.; Glaser, J. *Eur. J. Inorg. Chem.* **2001**, *1311*.
- (44) Maliarik, M.; Glaser, J.; Tóth, I. *Inorg. Chem.* **1998**, *37*, 5452.
- (45) Maliarik, M.; Berg, K.; Glaser, J.; Sandström, M.; Tóth, I. *Inorg. Chem.* **1998**, *37*, 2910.
- (46) Maliarik, M.; Glaser, J.; Tóth, I.; da Silva, M. W.; Zékány, L. *Eur. J. Inorg. Chem.* **1998**, *565*.
- (47) de Silva, N.; Fry, C. G.; Dahl, L. F. *Dalton Trans.* **2006**, 1051.
- (48) Studnichenko, R.; Sterenberg, B. T.; Bradford, A. M.; Jennings, M. C.; Puddephatt, R. J. *J. Chem. Soc., Dalton Trans.* **2002**, 1212.
- (49) Ezomo, O. J.; Mingos, D. M. P.; Williams, I. D. *J. Chem. Soc., Chem. Commun.* **1987**, 924.
- (50) Díez, A.; Forniés, J.; Gómez, J.; Lalinde, E.; Martín, A.; Moreno, M. T.; Sánchez, S. *Dalton Trans.* **2007**, 3653.

(Pt^{II}–Tl^I),⁵⁸ and (Pt^{II}–Tl^{III}),^{28,36,41–46,59–61} although in most cases, particularly in the latter ones, electronic redistribution makes it difficult, if not impossible, to assign oxidation states.

Given our recent interest in the luminescence behavior of heteropolynuclear platinum(II) complexes containing alkynyl ligands, different types of platinum–thallium complexes have recently been synthesized in our laboratory. Thus, homoleptic derivatives [Pt(C≡CR)₄]^{2–} (R = Ph, ^tBu, SiMe₃, Tol, 1-Naph) react with Tl^I salts affording sandwich hexanuclear luminescent clusters of the type [Pt₂Tl₄(C≡CR)₈]_n,^{25,27} in which the Tl^I centers show a strong bonding preference toward the electron rich alkynyl entities (B, Chart 1). However, by employing the substrate [Pt(C≡C–4-CF₃C₆H₄)₄]^{2–} containing the electron withdrawing substituent (R = 4-CF₃C₆H₄), the basic platinum center effectively competes with the alkynyl fragments showing a stronger preference for the Tl^I center. In this case, supramolecular columnar species [PtTl₂(C≡C–4-CF₃C₆H₄)₄(acetone)S]_∞ (S = acetone, dioxane)²⁵ containing two Pt–Tl bonds and stabilized by secondary Tl^I⋯(η²-acetylenic) interactions (C, Chart 1) were formed. Similar reactions with heteroleptic *cis*- or *trans*-[Pt(C₆F₅)₂(C≡CR)₂]^{2–} (R = Ph, ^tBu) also afforded complete neutralization, generating analogous six-coordinated platinum entities with two direct Pt–Tl bonds that dimerize (*cis*)²⁶ or polymerize (*trans*)³⁰ through secondary Tl–alkynyl(C_α) contacts. However, starting from (NBu₄)₂[Pt(C₆F₅)₄], even in presence of an excess of Tl^I, the corresponding PtTl₂ complex cannot be formed. Instead, we have obtained a diamagnetic trinuclear complex (NBu₄)₃[Tl{Pt(C₆F₅)₄}₂] (D, Chart 1) and two different anionic [Pt–Tl]_∞ chain systems, (NBu₄)_∞[Tl{Pt(C₆F₅)₄}]_∞ and (NBu₄)_∞[Tl{Pt(C₆F₅)₄}]_∞⋅{(NBu₄)(PF₆)_∞} (E, Chart 1), formed by alternate anionic fragments [Pt(C₆F₅)₄]^{2–} and naked Tl^I centers joined through lineal Pt–Tl bonds.²⁴ Of particular interest in this area is the paramagnetic trinuclear complex Pt^{II}–Tl^{II}, (NBu₄)₂[Tl{Pt(C₆F₅)₄}₂],⁵⁸ obtained by reaction of (NBu₄)₂[Pt(C₆F₅)₄] and [Tl(μ-Cl)(C₆F₅)₂]₂ (F, Chart 1).

Both experimental work and theoretical calculations indicate that the metallophilic Pt^{II}–Tl^I interaction in the final structures, as well as their optical properties, can be modified by varying the nature and stoichiometry of the anionic platinum substrates.^{24,25,31,51} Because alkynyl (C≡CR[–]) and

cyanide (CN[–]) groups are isoelectronic, we considered it of interest to prepare the heteroleptic cyano-pentafluorophenyl platinum substrates (NBu₄)₂[*trans*-Pt(C₆F₅)₂(CN)₂], (NBu₄)₂[*cis*-Pt(C₆F₅)₂(CN)₂], and (NBu₄)₂[*cis*-Pt(C₆F₅)₂(CN)-(PPh₂C≡CPh)]⁶² to investigate their reactivity toward Tl^I salts. We report here the preparation, X-ray single-crystal characterization, and photophysical properties of two extended structures (2D- [*trans,trans,trans*-Tl₂{Pt(C₆F₅)₂(CN)₂}⋅(CH₃COCH₃)₂]_n [**4**⋅(CH₃COCH₃)₂]_n and 1D- [Tl{Tl{*cis*-Pt(C₆F₅)₂(CN)₂}⋅(H₂O)}_n [**5**⋅(H₂O)]_n) and a discrete associated dimer [Tl{*cis*-Pt(C₆F₅)₂(CN)(PPh₂C≡CPh)}₂] [**6**]₂, based on Pt^{II}–Tl^I interactions.

Experimental Section

General procedures and preparation of (NBu₄)₂[*trans*-Pt(C₆F₅)₂(CN)₂] **1** and (NBu₄)₂[*cis*-Pt(C₆F₅)₂(CN)₂] **2** are described in the Supporting Information.

Preparation of [*trans,trans,trans*-Tl₂{Pt(C₆F₅)₂(CN)₂}] **4.** TIPF₆ (0.210 g, 0.600 mmol) was added to a solution of (NBu₄)₂[*trans*-Pt(C₆F₅)₂(CN)₂] **1** (0.320 g, 0.300 mmol) (2:1 molar ratio) in acetone (15 mL) at room temperature, and a white solid began to precipitate. After 4 h of stirring, the resulting white solid was filtered off and washed with acetone (0.238 g, 80% yield). Anal. Calcd for C₁₄F₁₀N₂PtTl₂: C, 16.99; N, 2.83. Found: C, 16.60; N, 3.01. MS (ES[–]): *m/z* 785 [M – Tl][–] 100%; 582 [M – 2Tl][–] 20%; 555 [Pt(C₆F₅)₂(CN)][–] 25%; 414 [Pt(C₆F₅)(CN)₂][–] 38%. IR (Nujol, cm^{–1}): ν(CN) 2102 (vs); ν(C₆F₅)_{X-sens} 775 (vs). Λ_M (5 × 10^{–4} M acetonitrile solution): 202.5 Ω^{–1}·cm²·mol^{–1}. Λ_M (5 × 10^{–4} M acetone solution): 121.5 Ω^{–1}·cm²·mol^{–1}. ¹⁹F NMR (282.4 MHz, CD₃COCD₃, 293 K): δ –112.6 (dm, ³J_{O-F-Pt} ≈ 290 Hz, 4o-F); –166.0 (t, 2p-F); –166.3 (m, 4m-F).

Preparation of [Tl{Tl{*cis*-Pt(C₆F₅)₂(CN)₂}]} **5.** The oily product (NBu₄)₂[*cis*-Pt(C₆F₅)₂(CN)₂] **2** (0.172 mmol) in acetone (15 mL) was treated with TIPF₆ (0.120 g, 0.344 mmol; 1:2 molar ratio). After 2 h of stirring, evaporation to a small volume caused the crystallization of **5** as a light yellow solid (0.130 g, 76% yield). Anal. Calcd for C₁₄F₁₀N₂PtTl₂: C, 16.99; N, 2.83. Found: C, 16.71; N, 3.13. MS (ES[–]): *m/z* 937 [M – 2CN][–] 3%; 823 [M – C₆F₅][–] 2%; 785 [M – Tl][–] 100%; 582 [M – 2Tl][–] 8%; 555 [Pt(C₆F₅)₂(CN)][–] 26%; 414 [Pt(C₆F₅)(CN)₂][–] 21%. IR (Nujol, cm^{–1}): ν(CN) 2125 (vs), 2112 (vs); ν(C₆F₅)_{X-sens} 798 (s); 788 (s). Λ_M (5 × 10^{–4} M acetonitrile solution): 154 Ω^{–1}·cm²·mol^{–1}. Λ_M (5 × 10^{–4} M acetone solution): 127.1 Ω^{–1}·cm²·mol^{–1}. ¹⁹F NMR (282.4 MHz, CD₃COCD₃): δ (293 K) –114.6 (dm, ³J_{O-F-Pt} ≈ 330 Hz, 4o-F); –164.9 (t, 2p-F); –166.0 (m, 4m-F); δ (193 K) –114.3 (s br, ³J_{O-F-Pt} ≈ 310 Hz, 4o-F); –163.2 (m, 2p-F); –164.8 (m, 4m-F).

Preparation of [Tl{*cis*-Pt(C₆F₅)₂(CN)(PPh₂C≡CPh)}] **6.** A solution of (NBu₄)₂[*cis*-Pt(C₆F₅)₂(CN)(PPh₂C≡CPh)] **3**⁶² (0.133 g, 0.123 mmol) in acetone (15 mL) was treated with TIPF₆ (0.043 g, 0.123 mmol) and a white solid was precipitated. After 48 h of stirring the solid **6** was filtered off (0.069 g, 54% yield). Anal. Calcd for C₃₃H₁₅F₁₀NPPtTl (M): C, 37.90; H, 1.45; N, 1.34. Found: C, 38.01; H, 1.46; N, 1.16. MS (ES[–]): *m/z* 842 [M – Tl][–] 100%. MS (ES⁺): *m/z* 1047 [M + H]⁺ 26%; 881 [M – C₆F₅ + 2H]⁺ 12%; 675 [M – C₆F₅ – Tl]⁺ 72%. IR (Nujol, cm^{–1}): ν(C≡C) 2177 (m), 2167 (m); ν(CN) 2116 (s), 2104 (s); ν(C₆F₅)_{X-sens} 797 (m), 786 (m). Λ_M (5 × 10^{–4} M acetonitrile solution): 120.5 Ω^{–1}·cm²·mol^{–1}. Λ_M (5 × 10^{–4} M acetone solution): 133.2 Ω^{–1}·cm²·mol^{–1}. ¹H NMR

(51) Maliarik, M.; Nagle, J. K.; Ilyukhin, A.; Murashova, E.; Mink, J.; Skripkin, M.; Glaser, J.; Kovacs, M.; Horváth, A. *Inorg. Chem.* **2007**, *46*, 4642.

(52) Wu, G.; Wang, D. *J. Cluster Sci.* **2007**, *18*, 406.

(53) Stork, J. R.; Olmstead, M. M.; Fettingner, J. C.; Balch, A. L. *Inorg. Chem.* **2006**, *45*, 849.

(54) Stork, J. R.; Olmstead, M. M.; Balch, A. L. *J. Am. Chem. Soc.* **2005**, *127*, 6512.

(55) Song, H. B.; Zhang, Z. Z.; Hui, Z.; Che, C. M.; Mak, T. C. W. *Inorg. Chem.* **2002**, *41*, 3146.

(56) Quadrelli, E. A.; Davies, J. E.; Johnson, B. F. G.; Feeder, N. *Chem. Commun.* **2000**, 1031.

(57) Renn, O.; Lippert, B.; Mutikainen, I. *Inorg. Chim. Acta* **1993**, *208*, 219.

(58) Usón, R.; Fornies, J.; Tomás, M.; Garde, R.; Alonso, P. J. *J. Am. Chem. Soc.* **1995**, *117*, 1837.

(59) Nagy, P.; Józsa, R.; Fábrián, I.; Tóth, I.; Glaser, J. *J. Mol. Liq.* **2005**, *118*, 195.

(60) Ma, G.; Kritikos, M.; Maliarik, M.; Glaser, J. *Inorg. Chem.* **2004**, *43*, 4328.

(61) Ma, G.; Fischer, A.; Glaser, J. *Eur. J. Inorg. Chem.* **2002**, 1307.

(62) Fornies, J.; García, A.; Gil, B.; Lalinde, E.; Moreno, M. T. *Dalton Trans.* **2004**, 3854.

Table 1. Crystal Data and Structure Refinement Details for **1**·2H₂O, **[4**·(CH₃COCH₃)₂]_n, **[5**·H₂O]_n, and **[6**·(CH₃COCH₃)₂]

	1 ·2H ₂ O	[4 ·(CH ₃ COCH ₃) ₂] _n	[5 ·H ₂ O] _n	[6 ·(CH ₃ COCH ₃) ₂]
empirical formula	C ₉₂ H ₁₄₄ F ₂₀ N ₈ O ₄ Pt ₂	C ₂₀ H ₁₂ F ₁₀ N ₂ O ₂ Pt ₂	C ₁₄ F ₁₀ N ₂ OPt ₂	C ₃₆ H ₂₁ F ₁₀ NOPt ₂
formula weight	2196.33	1106.15	1005.99	1103.97
temperature (K)	223(1)	173(1)	173(1)	173(1)
wavelength (Å)	0.71073	0.71073	0.71073	0.71073
crystal system	monoclinic	monoclinic	tetragonal	triclinic
space group	<i>P</i> 2 ₁ / <i>c</i>	<i>P</i> 2 ₁ / <i>c</i>	<i>I</i> 4 ₁ / <i>a</i>	<i>P</i> $\bar{1}$
<i>a</i> (Å); α (°)	16.3754(3); 90	12.5170(2); 90	26.0430(6); 90	10.3190(2); 66.3250(10)
<i>b</i> (Å); β (°)	15.4918(3); 96.7280(10)	7.50000(10); 101.7750(10)	26.0430(6); 90	13.0280(2); 75.2750(10)
<i>c</i> (Å); γ (°)	20.2262(5); 90	13.4070(3); 90	12.2720(3); 90	15.4547(2); 69.3390(10)
<i>V</i> (Å ³); <i>Z</i>	5095.74(19); 2	1232.13(4); 2	8323.3(3); 16	1765.02(5); 2
calcd density (Mg/m ³)	1.431	2.982	3.211	2.077
abs correction (mm ⁻¹)	2.828	18.806	22.250	8.646
<i>F</i> (000)	2240	984	6976	1032
crystal size (mm ³)	0.25 × 0.25 × 0.10	0.50 × 0.10 × 0.10	0.15 × 0.10 × 0.05	0.35 × 0.15 × 0.05
2 θ range (°)	1.25 to 27.48	3.13 to 27.48	2.41 to 27.87	2.73 to 27.91
index ranges	14 ≤ <i>h</i> ≤ 21, −20 ≤ <i>k</i> ≤ 20, −26 ≤ <i>l</i> ≤ 26	0 ≤ <i>h</i> ≤ 16, 0 ≤ <i>k</i> ≤ 9, −17 ≤ <i>l</i> ≤ 16	0 ≤ <i>h</i> ≤ 34, −23 ≤ <i>k</i> ≤ 24, −0 ≤ <i>l</i> ≤ 16	0 ≤ <i>h</i> ≤ 13, −15 ≤ <i>k</i> ≤ 17, −19 ≤ <i>l</i> ≤ 20
no. reflections collected	58677	2790	4970	8421
independent reflections	11645 [<i>R</i> (int) = 0.0834]	2790 [<i>R</i> (int) = 0.0000]	4970 [<i>R</i> (int) = 0.0000]	8421 [<i>R</i> (int) = 0.0000]
data/restraints/parameters	11645/12/525	2790/0/171	4970/0/271	8421/0/462
goodness of fit on <i>F</i> ² ^a	1.027	1.022	1.086	1.005
final <i>R</i> indices [<i>I</i> > 2 σ (<i>I</i>)] ^a	<i>R</i> 1 = 0.0593, <i>wR</i> 2 = 0.1491	<i>R</i> 1 = 0.0328, <i>wR</i> 2 = 0.0774	<i>R</i> 1 = 0.0412, <i>wR</i> 2 = 0.0863	<i>R</i> 1 = 0.0392, <i>wR</i> 2 = 0.0860
<i>R</i> indices (all data) ^a	<i>R</i> 1 = 0.1380, <i>wR</i> 2 = 0.1857	<i>R</i> 1 = 0.0427, <i>wR</i> 2 = 0.0817	<i>R</i> 1 = 0.0667, <i>wR</i> 2 = 0.0956	<i>R</i> 1 = 0.0627, <i>wR</i> 2 = 0.0943
largest diff. peak and hole	0.954 and −1.372 e Å ⁻³	1.669 and −2.462 e Å ⁻³	0.825 and −1.608 e Å ⁻³	1.513 and −3.203 e Å ⁻³

^a *R*1 = $\sum(|F_o| - |F_c|)/\sum|F_o|$; *wR*2 = $[\sum w(F_o^2 - F_c^2)^2/\sum wF_o^2]^{1/2}$; goodness of fit = $\{\sum[w(F_o^2 - F_c^2)^2]/(N_{\text{obs}} - N_{\text{param}})\}^{1/2}$; *w* = $[\sigma^2(F_o^2) + (g_1P)^2 + g_2P]^{-1}$; *P* = $[\max(F_o^2, 0) + 2F_c^2]/3$.

(300.1 MHz, CD₃COCD₃, 293 K): δ 7.99 (m, 4H); 7.51 (m, 5H); 7.44 (m, 6H) (Ph). ¹³C{¹H} NMR (100.6 MHz, CD₃COCD₃, 293 K): δ 148.9 (dm, ¹*J*_{C-F} ≈ 230 Hz, C₆F₅); 138.2 (dm, ¹*J*_{C-F} ≈ 240 Hz, C₆F₅); 135.0 (d, ²*J*_{C-P} = 13 Hz, ³*J*_{C-Pt} = 20 Hz, *o*-C, PPh₂); 133.9 (d, ¹*J*_{C-P} = 60.9 Hz, ²*J*_{C-Pt} = 22 Hz, *i*-C, PPh₂); 133.7 (s br, *o*-C, Ph); 132.8 (d, ⁴*J*_{C-P} = 2.1 Hz, *p*-C, PPh₂); 132.1 (s, *p*-C, Ph); 130.5 (s, *m*-C, Ph); 130.3 (d, ³*J*_{C-P} = 11.3 Hz, *m*-C, PPh₂); 122.7 (d, ³*J*_{C-P} = 2.9 Hz, *i*-C, Ph); 109.4 (d, ²*J*_{C-P} = 14.1 Hz, C_β, PC_α≡C_βPh); 82.4 (d, ¹*J*_{C-P} = 98.2 Hz, ²*J*_{C-Pt} = 27.7 Hz, C_α, PC_α≡C_βPh). ¹⁹F NMR (282.4 MHz, CD₃COCD₃): δ (298 K) −115.8 (m, ³*J*_{o-F-Pt} ≈ 390 Hz, 2*o*-F); −116.0 (m, ³*J*_{o-F-Pt} ≈ 365 Hz, 2*o*-F); −164.6 (t, 1*p*-F); −165.4 (t, 1*p*-F); −166.2 (m, 4*m*-F); δ (193 K) −115.9 (m, ³*J*_{o-F-Pt} ≈ 360 Hz, 4*o*-F); −163.1 (t, 1*p*-F); −164.2 (t, 1*p*-F); −164.9 (m, 4*m*-F). ³¹P{¹H} NMR (121.5 MHz, CD₃COCD₃, 293 K): δ −7.39 (s, ¹*J*_{P-Pt} ≈ 2485 Hz). ¹⁹⁵Pt NMR (85.6 MHz, CD₃COCD₃, 293 K): δ −4466.9 (dtt, ¹*J*_{Pt-P} ≈ 2440 Hz, ³*J*_{Pt-o-F} ≈ 370, 440 Hz).

X-ray Crystallography. Crystal data and other details of the structure analyses are presented in Table 1. Colorless (**1**, **6**) crystals were obtained by slow diffusion of *n*-hexane into a dichloromethane (**1** at −30 °C) or acetone (**6** at room temperature) solution of the corresponding complexes. For complex **5** one molecule of water and for complexes **4** and **6**, two and one molecules of acetone were found, respectively, in the asymmetric unit. Complex **1** crystallizes with two independent but very similar half-molecules and two molecules of water per asymmetric unit. The diffraction measurements were made on a NONIUS κ -CCD area-detector diffractometer, using graphite-monochromated Mo K α radiation. Images were processed using the DENZO and SCALEPACK suite of programs,⁶³ carrying out the absorption correction at this point for complexes **4–6**. The structure of **1**·2H₂O was solved by direct methods, the structure of **[6**·(CH₃COCH₃)₂] was solved by the Patterson method using, in both cases, the SHELXS-97 program,⁶⁴ and the absorption correction was performed using MULTISCAN

(**1**·2H₂O).⁶⁵ The structures of **[4**·(CH₃COCH₃)₂]_n and **[5**·H₂O]_n were solved by the Patterson and Fourier methods using the DIRDIF92 program.⁶⁶ All structures were refined by full-matrix least-squares on *F*² with SHELXL-97.⁶⁷ All non-hydrogen atoms were assigned anisotropic displacement parameters, and all hydrogen atoms were constrained to idealized geometries fixing isotropic displacement parameters of 1.2 times the *U*_{iso} value of their attached carbon for the phenyl and methyne hydrogens and 1.5 for the methyl groups. For complex **1**·2H₂O one molecule of NBu₄⁺ was modeled adequately. For complexes **[4**·(CH₃COCH₃)₂]_n and **[6**·(CH₃COCH₃)₂]_n residual peaks bigger than 1 e Å⁻³ close to their respective metal atoms have been observed, but with no chemical meaning.

Results and Discussion

Synthesis and Characterization. With the aim of comparing the metallophilic affinity of Tl^I toward anionic platinum fragments containing simultaneously C₆F₅ and CN⁻ groups with that of the homoleptic [PtX₄]²⁻ (X = C₆F₅, CN, C≡CR) or mixed [*trans*-Pt(C₆F₅)₂(C≡CBu^t)₂]²⁻ and *cis*-[Pt(C₆F₅)₂(C≡CPh)₂]²⁻ derivatives, we have prepared the related mixed (NBu₄)₂[*trans*-Pt(C₆F₅)₂(CN)₂] **1** and (NBu₄)₂[*cis*-Pt(C₆F₅)₂(CN)₂] **2** substrates and examined their reactions with TIPF₆. The synthetic work is summarized in Scheme 1. The mononuclear complexes **1** (white solid) and **2** (as an oil) are easily prepared by displacement of the tetrahydrothiophene ligands on the corresponding *trans*- or *cis*-[Pt(C₆F₅)₂(tth)₂] derivatives with two equivalents of

(64) Sheldrick, G. M. *SHELX-97, Program for the Solution of Crystal Structures*; University of Göttingen: Göttingen, Germany, 1997.

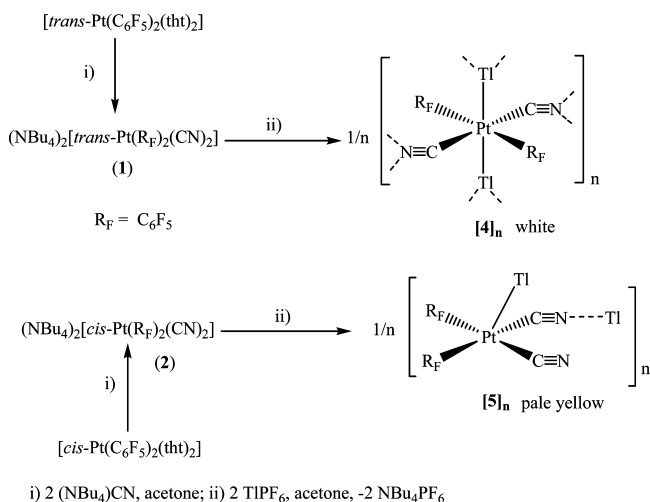
(65) Blessing, R. H. *Acta Crystallogr.* **1995**, *A51*, 33.

(66) Beursken, P. T.; Beursken, G.; Bosman, W. P.; de Gelder, R.; García-Granda, S.; Gould, R. O.; Smith, J. M. M.; Smykalla, C. *The DIRDIF92 program system*; Technical Report of the Crystallography Laboratory; University of Nijmegen: The Netherlands, 1992.

(67) Sheldrick, G. M. *SHELX-97: Program for Crystal Structure Refinement*; University of Göttingen: Göttingen, Germany, 1997.

(63) Otwinowski, Z.; Minor, W. In *Methods Enzymol.*; Carter, C. V., Jr., Sweet, R. M., Eds.; Academic Press: New York, 1997; Vol. 276A, p 307.

Scheme 1



$(\text{NBu}_4)\text{CN}$ (see Supporting Information). Both complexes have been characterized by usual analytical and spectroscopic techniques and in the case of **1** by an X-ray crystallographic study (Supporting Information, Figures S1 and S2). Details of the structure including a table with selected bonding parameters are given in Supporting Information, Table S1.

As is shown in Scheme 1, treatment of the dianionic species $(\text{NBu}_4)_2[trans\text{-Pt}(\text{C}_6\text{F}_5)_2(\text{CN})_2]$ **1** and $(\text{NBu}_4)_2[cis\text{-Pt}(\text{C}_6\text{F}_5)_2(\text{CN})_2]$ **2** with TIPF_6 (1:2) in acetone results in the formation of two solids of identical stoichiometry $[\text{Ti}_2\{\text{Pt}(\text{C}_6\text{F}_5)_2(\text{CN})_2\}]_n$ but different colors (**4**, white, and **5**, pale yellow). Crystals of both products were obtained; in the case of the *trans* derivative as the solvate $4 \cdot (\text{CH}_3\text{COCH}_3)_2$ generated by slow diffusion of an acetone solution of TIPF_6 into an acetone solution of **1**, and in the case of the *cis* as $5 \cdot (\text{H}_2\text{O})$ by slow evaporation of an ethanolic solution of the crude solid. Crystallographic characterization of $4 \cdot (\text{CH}_3\text{COCH}_3)_2$ and of $5 \cdot (\text{H}_2\text{O})$ have shown that the white solid generates a two-dimensional (2D) framework of stoichiometry $[trans,trans,trans\text{-Ti}_2\{\text{Pt}(\text{C}_6\text{F}_5)_2(\text{CN})_2\} \cdot (\text{CH}_3\text{COCH}_3)_2]_n$ ($[4 \cdot (\text{CH}_3\text{COCH}_3)_2]_n$) while the pale yellow solid forms an extended 1D helicoidal chain $\{\text{Ti}[\text{Ti}\{cis\text{-Pt}(\text{C}_6\text{F}_5)_2(\text{CN})_2\} \cdot (\text{H}_2\text{O})]_n\}$ ($[5 \cdot (\text{H}_2\text{O})]_n$). The asymmetric unit of $[4 \cdot (\text{CH}_3\text{COCH}_3)_2]_n$ contains the unit $[\text{Ti}\{\text{Pt}(\text{C}_6\text{F}_5)_2(\text{CN})_2\}]$ and one acetone molecule (see Figure 1a), which generates the hexanuclear unit $[trans,trans,trans\text{-Ti}_2\{\text{Pt}(\text{C}_6\text{F}_5)_2(\text{CN})_2\} \cdot (\text{CH}_3\text{COCH}_3)_2]_2$, by applying the corresponding symmetry operations. The molecular structure reveals a pseudooctahedral environment around the platinum center (Figure 1b, Table 2), formed by two *trans* C_{ipso} from the C_6F_5 groups, two *trans* cyanide groups and two *trans* donor-acceptor Pt-Tl bonds (Ti-Pt-Ti 180°). The Pt-Tl distance (3.2087(3) Å) compares well with those observed in other systems with $\text{Pt}^{\text{II}}\text{-Ti}^{\text{I}}$ interactions (2.7961(7)–3.5675(5) Å) ($<$ than the sum of van der Waals radii 3.68 Å),^{23–27,29,34,35,37,50–57} and it is only slightly longer than the sum of the metallic radii (3.08 Å).⁶⁸ A view of the extended lattice (Supporting Information, Figure S3) shows that each

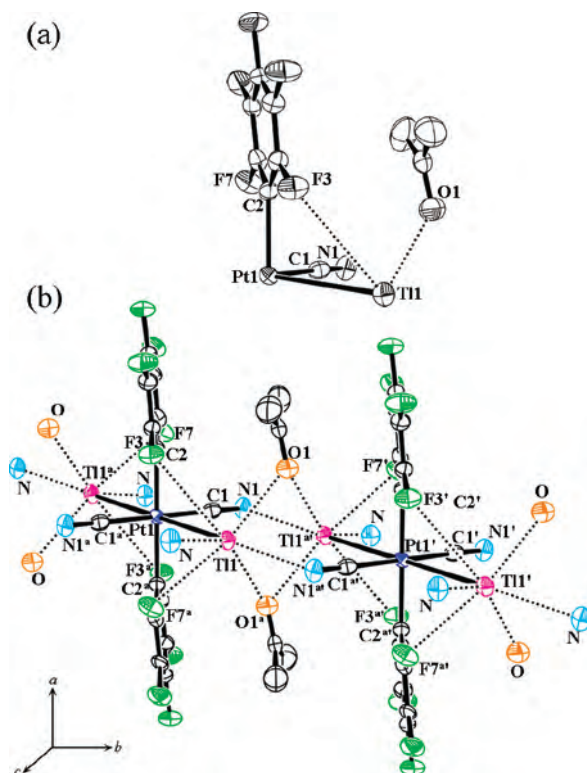


Figure 1. Molecular structure of $[trans,trans,trans\text{-Ti}_2\{\text{Pt}(\text{C}_6\text{F}_5)_2(\text{CN})_2\}(\text{CH}_3\text{COCH}_3)_2]_n$ $[4 \cdot (\text{CH}_3\text{COCH}_3)_2]_n$ (a) ORTEP view of the asymmetric unit and (b) two molecules of $[trans,trans,trans\text{-Ti}_2\{\text{Pt}(\text{C}_6\text{F}_5)_2(\text{CN})_2\}(\text{CH}_3\text{COCH}_3)_2]_n$ showing secondary interactions. Ellipsoids are drawn at 50% probability level. Hydrogen atoms are omitted for clarity.

Table 2. Selected Bond Distances (Å) and Angles (°) for $[trans,trans,trans\text{-Ti}_2\{\text{Pt}(\text{C}_6\text{F}_5)_2(\text{CN})_2\} \cdot (\text{CH}_3\text{COCH}_3)_2]_n$ $[4 \cdot (\text{CH}_3\text{COCH}_3)_2]_n$ ^a

Pt(1)–Ti(1)	3.2087(3)	Ti(1)···O(1a)	3.039(6)
Pt(1)–C(1)	1.987(7)	Ti(1)···O(1)	2.896(7)
Pt(1)–C(2)	2.082(7)	Ti(1)···F(3)	3.311(4)
C(1)–N(1)	1.146(9)	Ti(1)···F(7a)	2.970(5)
Ti(1)–N(1a')	2.783(6)	Ti(1)–N(1)	2.828(6)
Ti(1)–Pt(1)–Ti(1a)	180.0	Ti(1)–Pt(1)–C(2a)	84.94(18)
C(1)–Pt(1)–C(2a)	89.7(3)	Ti(1)–N(1a)–C(1a)	115.9(5)
C(1)–Pt(1)–C(2)	90.3(3)	Ti(1a)–N(1)–C(1)	120.3(45)
Ti(1)–Pt(1)–C(1)	82.53(19)	N–Ti–N	100.04(11)
Ti(1)–Pt(1)–C(1a)	97.47(19)	Ti–N–Ti	121.42(19)
Ti(1)–Pt(1)–C(2)	95.06(18)	Pt–Ti–N	102.67(11), 156.82(12)

^a Symmetry transformations used to generate equivalent atoms are: 1) $-x, -y, -z$; 2) $x, y - 1, -z$; 3) $-x, -y + 1, -z$; 4) $x, -y + 1/2, -z + 1/2$; 5) $x, y + 1, z$; 6) $x, -y + 1/2, -z - 1/2$.

Tl atom in the octahedral unit is coordinated additionally to two N atoms of the two CN^- ligands, each one from a neighboring unit, generating a layered structure. The $\text{Ti} \cdots \text{N}(\text{CN})$ contacts $[\text{Ti}(1) - \text{N}(1a') 2.783(6) \text{ \AA}, \text{Ti}(1) - \text{N}(1) 2.828(6) \text{ \AA}]$ are comparable to those observed in related derivatives containing cyanide groups such as $[\text{PtTi}_2(\text{CN})_4]$ (2.80–3.04 Å),^{31,35,51} $[\text{Ti}\{\text{Pt}(\text{C}_4\text{H}_9\text{N}_4)(\text{CN})_2\}]_n$ (red polymorph 2.691(9) Å),⁵⁴ or in $[5 \cdot (\text{H}_2\text{O})]_n$ (2.699(9)–2.879(9) Å). As a consequence, the CN ligand shows an unusual $\mu_3\text{-}\kappa\text{C}:\kappa\text{N}:\kappa\text{N}$ bridging mode, C-bound to the platinum center and N-contacting to two thallium atoms.^{69–71} As can be observed in Figure 1b, the orientation of the C_6F_5 rings allows the formation of $o\text{-F} \cdots \text{Ti}$ secondary contacts. The $\text{Ti} \cdots \text{F}$

(68) Winter, M. *WebElement*TM; the Periodic Table on the www.; University of Sheffield: U.K.; <http://www.webelements.com> (accessed Oct 2007).

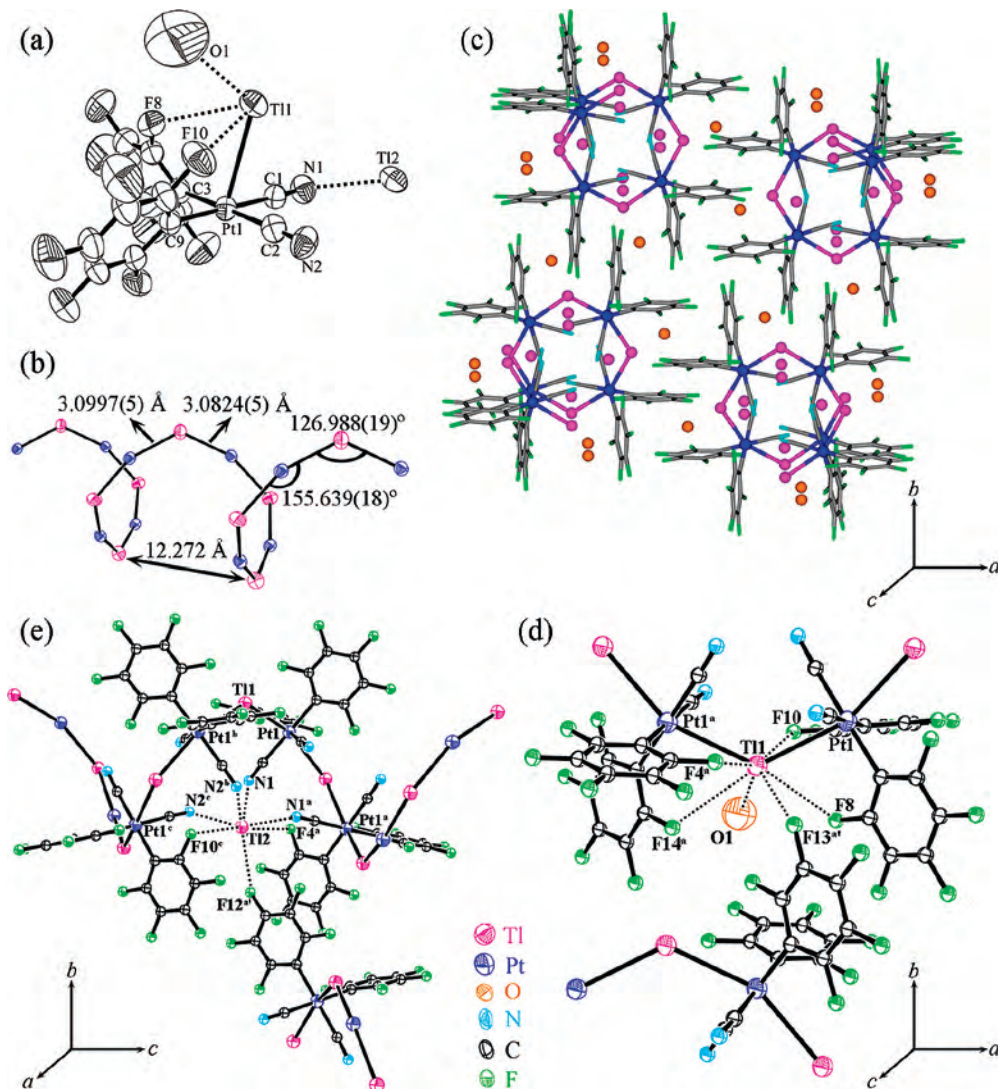


Figure 2. Molecular structure of $\{Tl[Tl\{cis\text{-}Pt(C_6F_5)_2(CN)_2\} \cdot (H_2O)]_n [5 \cdot (H_2O)]_n$. (a) ORTEP view of the asymmetric unit (ellipsoids at the 50% probability level). (b) Schematic view of the core Pt–Tl(1) in the helical chain. (c) View of four helical chains packing diagram projected down the crystallographic c axis. (d) ORTEP view of Tl(1) environment and (e) ORTEP view of Tl(2) environment.

distances (range 2.970(5)–3.311(4) Å), although lower than the sum of van der Waals radii of Tl and F (3.43 Å),⁶⁸ are clearly larger than those measured in related systems such as $[\{Pt(C_6F_5)_4\}_2Tl]^{3-}$ (2.883(5)–3.065(12) Å) or $[\{Pt(C_6F_5)_4\}Tl]_n^{n-}$ (2.956 Å).²⁴ As a consequence, these interactions are easily lost in solution, even at low temperature. Finally, it should be noted that the location of the acetone molecules above and below the final layer enables each thallium center to also establish weak interactions with the oxygen atoms of two acetones, which are acting as bridging groups [O(1/1a)–Tl(1/1a) 2.896(7) Å; O(1/1a)–Tl(1a/1) 3.039(6) Å] (Figure 1). These distances are somewhat smaller than those found in other complexes where the acetone molecules are also weakly bonded to thallium.^{25,26,30,72}

Several views of the molecular structure of $[5 \cdot (H_2O)]_n$ are shown in Figure 2 (see also Table 3). The comparison

Table 3. Selected Bond Distances (Å) and Angles (°) for $\{Tl[Tl\{cis\text{-}Pt(C_6F_5)_2(CN)_2\} \cdot (H_2O)]_n [5 \cdot (H_2O)]_n^a$

Pt(1) Environment			
Pt(1)–C(1)	1.987(10)	C(1)–Pt(1)–C(2)	90.8(4)
Pt(1)–C(2)	1.971(10)	C(1)–Pt(1)–C(3)	88.8(4)
Pt(1)–C(3)	2.067(9)	C(2)–Pt(1)–C(9)	88.8(4)
Pt(1)–C(9)	2.057(9)	C(3)–Pt(1)–C(9)	91.5(4)
N(1)–C(1)	1.142(12)	Pt(1)–C(1)–N(1)	177.6(9)
N(2)–C(2)	1.185(12)	Pt(1)–C(2)–N(2)	177.8(9)
Tl(1) Environment			
Tl(1)–Pt(1)	3.0997(5)	Tl(1)···F(8) _{ortho}	3.104(6)
Tl(1)–Pt(1a)	3.0824(5)	Tl(1)···F(10) _{ortho}	3.045(6)
Tl(1)–Pt(1)–Tl(1a)	155.639(18)	Tl(1)···F(4a) _{ortho}	3.038(8)
Pt(1)–Tl(1)–Pt(1a)	126.988(19)	Tl(1)···F(14a) _{ortho}	3.252(7)
Tl(1)···O(1)	3.228(4)	Tl(1)···F(13a') _{meta}	3.236(9)
Tl(2) Environment			
Tl(2)–N(1)	2.699(9)	Tl(2)···F(4a) _{ortho}	3.441(7)
Tl(2)–N(1a)	2.871(9)	Tl(2)···F(10c) _{ortho}	3.384(7)
Tl(2)–N(2b)	2.714(9)	Tl(1)···F(12a') _{para}	3.198(8)
Tl(2)–N(2c)	2.879(9)		

^a Symmetry transformations used to generate equivalent atoms are as follows: (1) $-y + 1/4, x - 1/4, z - 1/4$; (2) $y + 1/4, -x + 1/4, z + 1/4$.

between the structures of *trans*, $[4 \cdot (CH_3COCH_3)_2]_n$, and *cis*, $[5 \cdot (H_2O)]_n$, indicates that the change from a *trans* to a *cis* geometry of the C_6F_5 and CN ligands decreases the platinum

(69) Connelly, N. G.; Hicks, O. M.; Lewis, G. R.; Moreno, M. T.; Orpen, A. G. *J. Chem. Soc., Dalton Trans.* **1998**, 1913.

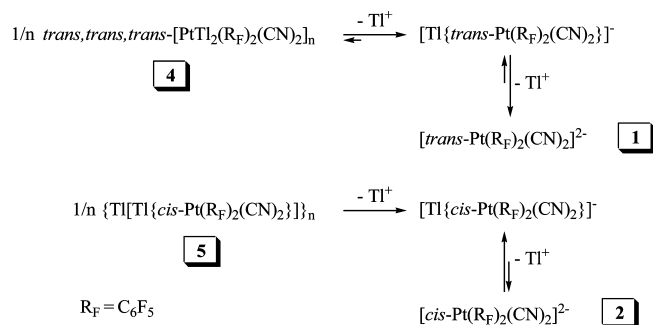
(70) Davies, R. P.; Hornauer, S. *Inorg. Chem.* **2005**, *1*, 51.

(71) Eaborn, C.; Hill, M. S.; Hitchcock, P. B.; Smith, J. D. *Organometallics* **2000**, *19*, 5780.

to thallium methallophilic interaction. In this case, the asymmetric unit contains the entity $[\text{Tl}_2\{\text{cis-Pt}(\text{C}_6\text{F}_5)_2(\text{CN})_2\}]$ with two different Tl centers and one water molecule. As is shown in Figure 2a, while the Tl(1) interacts directly with the platinum center, the second thallium center Tl(2) contacts through electrostatic interactions with the N(1) atom of one cyanide group. In this unit, the Pt–Tl(1) vector is perceptibly bent ($13.56(15)^\circ$) toward the cyanide ligands. By applying the corresponding symmetry operations, an extended helical $[-\text{Pt}-\text{Tl}(1)-\text{Pt}-\text{Tl}(1)-]_n^{n-}$ chain is generated by connection of the anionic $[\text{Pt}-\text{Tl}(1)(\text{R}_\text{F})_2(\text{CN})_2]^-$ motifs (Figure 2b). In the final chain, each platinum atom is coordinated to two thallium centers, with Pt–Tl(1) bond distances of 3.0824(5) and 3.0997(5) Å and angles at metals of $155.639(18)^\circ$ (Tl–Pt–Tl) and $126.988(19)^\circ$ (Pt–Tl–Pt). The Pt–Tl bond distances are shorter than that observed in the layer-type *trans* derivative $[\mathbf{4}\cdot(\text{CH}_3\text{COCH}_3)_2]_n$. As has been previously noted by Pyykkö for $[\text{Tl}_2\text{Pt}(\text{CN})_4]^{31}$ and by Balch and co-workers for $[\text{Tl}\{\text{Pt}(\text{C}_4\text{H}_9\text{N}_4)(\text{CN})_2\}]_n$,⁵³ the local interaction of Tl^I in complex **4** with the N atoms of the neighboring CN groups may be responsible for the longer Tl···Pt bond distance in this compound (3.2087(3) Å). In the *cis* derivative, $[\mathbf{5}\cdot(\text{H}_2\text{O})]_n$, the resulting helical chain is extended along the *c* axis and its translation is defined by eight metal atoms (four Pt and four Tl) with a long separation between equivalent metal atoms (Pt–Pt or Tl–Tl of 12.272 Å). This complex crystallizes in the centric group of $I4_1/a$ and is thus optically inactive. Crystals are composed of both P (right-handed) and M (left-handed) helices, affording an internal racemate. As is seen in Figure 2c, in which the projection of four helical chains is shown, the C_6F_5 groups are oriented to the external part of the chain while the cyanide ligands and Tl(2) metal centers are located in the internal part. The two different environments of both Tl centers are shown in Figures 2e (for Tl(2)) and 2d (for Tl(1)). The Tl(1) center, which is forming the helical chain (Figure 2d), is coordinated to two Pt centers and establishes secondary interactions with four *o*-fluorine atoms of the C_6F_5 groups of two adjacent “*cis*-Pt(C_6F_5)₂(CN)₂” units (3.038(8)–3.252(7) Å), the oxygen atom of the cocrystallization water molecule (Tl–O 3.228(4) Å) and the *m*-fluorine atom of a C_6F_5 ring of an adjacent chain [Tl(1)···F(13a') = 3.236(9) Å]. These contacts, albeit weak, presumably contribute to the stability of the packing. The Tl(2) center, inside the helical chain $[-\text{Pt}-\text{Tl}(1)-\text{Pt}-\text{Tl}(1)-]_n^{n-}$, (Figure 2e) is mainly stabilized by interaction with four nitrogen atoms of the cyanide groups, with Tl···N contacts in the range 2.699(9)–2.879(9) Å. These Tl(2)···N electrostatic interactions could be responsible for the distortion of linearity along the Pt–Tl(1)–Pt–Tl motif giving rise to the final helicoidal chain where the cyanide ligands are inside-oriented. Additionally, the Tl(2) atom interacts weakly with two *o*-fluorine atoms of the C_6F_5 ring of two adjacent units and a *p*-fluorine of the other adjacent helical chain (range Tl···F 3.198(8)–3.441(7) Å).

Both complexes **4** and **5** gave satisfactory elemental analysis for the microcrystalline solids isolated from the

Scheme 2



reactions. We noted that crystals of **4**·(CH₃COCH₃)₂ and **5**·(H₂O) lose the solvent molecules easily in contact with air. Their mass spectra (ES⁻) reveal the presence of a peak at *m/z* 785 corresponding to the bimetallic anion $[\text{PtTl}(\text{C}_6\text{F}_5)_2(\text{CN})_2]^-$ as the parent peak. The observation of one (**4**) or two (**5**) $\nu(\text{CN})/\nu(\text{C}_6\text{F}_5)_{\text{X-sens}}$ absorptions (2102/775 cm⁻¹ **4**; 2125, 2112/798, 788 cm⁻¹ **5**) confirms that the *trans* or *cis* geometry of the precursors is retained upon thallium coordination. Conductivity measurements in acetonitrile solution suggest that the thallium center is at least partially dissociated in solution, which is presumably a more widespread feature in the *trans* derivative **4** (202.5 Ω⁻¹·cm²·mol⁻¹, nearly 1:2 electrolyte) than in the *cis* **5** (154 Ω⁻¹·cm²·mol⁻¹, 1:1 electrolyte). The extent of the Pt–Tl dissociative process is lesser in acetone solvent, exhibiting values close to a 1:1 electrolyte for both derivatives (121.5 Ω⁻¹·cm²·mol⁻¹ **4**, 127.1 Ω⁻¹·cm²·mol⁻¹ **5**). Furthermore, the dissociation of the Pt–Tl bonds is reflected in the ¹⁹F NMR spectra (CD₃COCD₃), and no fluorine–thallium couplings are observed neither at room temperature nor at low temperature (193 K). Both derivatives (**4** and **5**) show at room temperature only one set of C_6F_5 signals (with the typical pattern of three signals 2:1:2). At low temperature (193 K) the spectrum for **4** is not modified, while for **5** a clear broadening of the *o*-fluorine was observed. Although the values of the chemical shift of the *o*-fluorine atoms in both complexes are very close to those observed in the corresponding precursors (see Experimental Section), the ³*J*_{*o*-F–Pt} coupling constants are notably smaller (290 Hz **4**/360 Hz **1** Δ = 70 Hz; 330 Hz **5**/410 Hz **2** Δ = 80 Hz). Probably, the dissociation of one Tl center occurs more easily than the dissociation of the second one, generating a fast equilibrium mainly between the monoanionic $[\text{Tl}\{\text{trans-/cis-}[\text{Pt}(\text{C}_6\text{F}_5)_2(\text{CN})_2]\}]^-$ and the dianionic $[\text{trans-/cis-Pt}(\text{C}_6\text{F}_5)_2(\text{CN})_2]^{2-}$ species (see Scheme 2). The perceptible decrease of the observed ³*J*_{*o*-F–Pt} values relative to the precursors **1** and **2** can be tentatively attributed to the presence of monoanionic $[\text{Tl}\{\text{Pt}(\text{C}_6\text{F}_5)_2(\text{CN})_2\}]^-$ fragments in solution.

In this same line of study, we decided to examine the reactivity of the monocyno complex (NBu₄)[*cis*-Pt(C_6F_5)₂(CN)(PPh₂C≡CPh)] **3**⁶² toward Tl(I). Complex **3** reacts with TlPF₆ in acetone (1:1) to give a white solid, whose dimeric formulation $[\text{Tl}\{\text{cis-Pt}(\text{C}_6\text{F}_5)_2(\text{CN})(\text{PPh}_2\text{C}\equiv\text{CPh})\}]_2$ [**6**]₂ (Scheme 3) was established by X-ray diffraction (Figure 3). Relevant bond distances and angles are shown in Table 4. The asymmetric unit in [**6**]₂ contains

(72) Fernández, E. J.; López de Luzuriaga, J. M.; Monge, M.; Olmos, M. E.; Perez, J.; Laguna, A. *J. Am. Chem. Soc.* **2002**, *124*, 5942.

Scheme 3

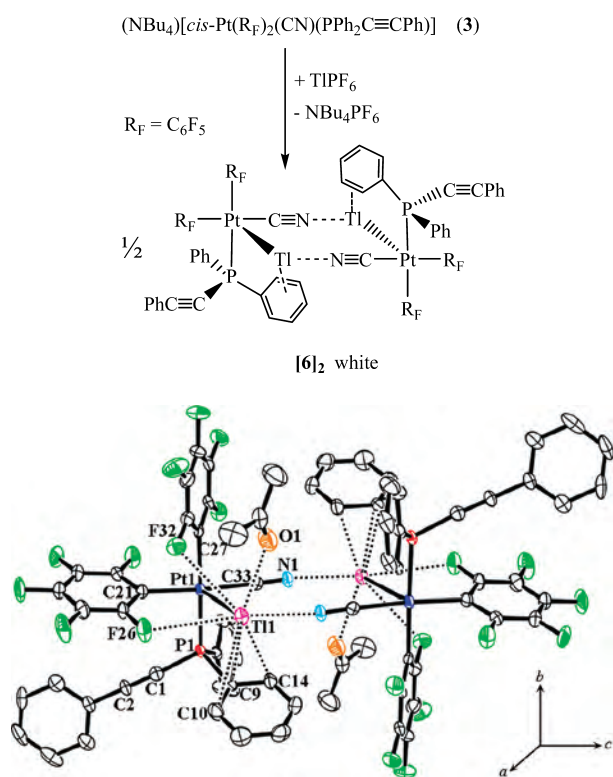


Figure 3. Dimeric disposition of the molecular structure of [Tl{*cis*-Pt(C₆F₅)₂(CN)(PPh₂C≡CPh)}·(CH₃COCH₃)₂] [6·(CH₃COCH₃)₂]. Ellipsoids are drawn at 50% probability level. Hydrogen atoms are omitted for clarity.

Table 4. Selected Bond Distances (Å) and Angles (°) for [Tl{*cis*-Pt(C₆F₅)₂(CN)(PPh₂C≡CPh)}·(CH₃COCH₃)₂] [6·(CH₃COCH₃)₂]^a

Pt(1)–Tl(1)	3.0756(3)	Tl(1)–N(1a)	2.690(5)
Pt(1)–C(21)	2.046(5)	Tl(1)···O(1)	2.825(6)
Pt(1)–C(27)	2.061(6)	Tl(1)···F(26)	3.294(3)
Pt(1)–P(1)	2.2818(15)	Tl(1)···F(32)	3.159(4)
Pt(1)–C(33)	2.006(6)	Tl(1)···C(9)	3.443(8)
C(33)–N(1)	1.135(7)	Tl(1)···C(10)	3.706(8)
C(1)–C(2)	1.204(8)	Tl(1)···C(14)	3.624(9)
C(33)–Pt(1)–C(27)	89.0(2)	Tl(1)–Pt(1)–C(33)	76.14(15)
C(21)–Pt(1)–C(27)	87.6(2)	Tl(1)–Pt(1)–C(21)	106.96(17)
C(33)–Pt(1)–P(1)	91.62(16)	Tl(1)–Pt(1)–C(27)	91.58(16)
C(21)–Pt(1)–P(1)	91.60(16)	Tl(1)–Pt(1)–P(1)	91.21(4)
Pt(1)–C(33)–N(1)	178.1(5)	Tl(1)–N(1a)–C(33a)	172.9(4)
P(1)–C(1)–C(2)	173.7(5)	Pt(1)–Tl(1)–N(1a)	108.57(10)
C(1)–C(2)–C(3)	179.0(7)		

^a Symmetry transformations used to generate equivalent atoms are $-x + 2, -y + 2, -z + 1$.

a [Tl{*cis*-Pt(C₆F₅)₂(CN)(PPh₂C≡CPh)}] unit and one acetone molecule and can be seen as a square pyramid in which the planar environment of the Pt^{II} forms the base of the pyramid and the Tl^I center the apical position. The Pt–Tl bond (3.0756(3) Å), similar to those found in [5·(H₂O)]_n, forms an angle with the normal to the coordination Pt^{II} plane of 15.36(12)°. This unit dimerizes by weak contacts between the Tl^I center and the N atom of the cyanide ligand of the next unit (Tl(1)–N = 2.690(5) Å), to form the tetranuclear complex [Tl{*cis*-Pt(C₆F₅)₂(CN)(PPh₂C≡CPh)}·(CH₃COCH₃)₂] [6·(CH₃COCH₃)₂]. As is shown in Figure 3, the thallium center establishes additional very weak contacts with two *o*-fluorine atoms [Tl(1)–F(26), F(32)

3.294(3) and 3.159(4) Å], the acetone molecule [Tl–O 2.825(6) Å], and with the π electronic density of one of the phenyl rings [C(9)–C(14)]. The distances between phenyl carbon atoms C(9), C(10), C(14), and Tl^I (3.443(8)–3.706(8) Å) are within the range observed for other compounds with π –Tl interactions,^{73–81} although they are slightly longer than those reported for [(PCH₂-ox)ClPtTl{ μ -(η^1 -CH₂, η^6 -C₆H₅)CH₂Ph}](PF₆) (3.015(5)–3.620(5) Å), which shows an η^6 -benzyl interaction.³⁷

In solution, the platinum–thallium bond is broken, and its spectroscopic data are similar to those of the precursor even at low temperature (193 K, see Experimental Section). In particular, the *o*-fluorine resonances, the ³J_{o-F–Pt} coupling constants and the ³¹P{¹H} and ¹³C{¹H} NMR spectra are essentially identical to those seen in 3.⁶² This fact and its behavior as a 1:1 electrolyte (acetone or acetonitrile) are consistent with a nearly complete dissociation of the Tl(I). The most remarkable spectroscopic feature is the splitting of the ν (C≡C) and ν (CN) stretching bands [ν (C≡C) 2177, 2167 cm⁻¹; ν (CN) 2116, 2104 cm⁻¹] in its IR spectrum with respect to the precursor 3 [ν (C≡C) 2177 cm⁻¹; ν (CN) 2117 cm⁻¹] (probably because of solid effects). Curiously, the ν (CN) absorptions do not shift toward higher frequencies, as was expected for a bridge CN⁻ group, suggesting that the interaction of the Tl(I) center with the CN⁻ group is rather weak, in agreement with the relatively long Tl···N(cyanide) distance found in the solid state (2.690(5) Å).

Photophysical Properties. Absorption spectra of precursors (1, 3) and heteropolynuclear Pt–Tl complexes (4–6) were obtained in acetonitrile solutions and in the solid state (Supporting Information, Figures S4–S6). In agreement with the complete rupture of the Pt–Tl bond in solution, the absorption spectra of the [Tl{*cis*-Pt(C₆F₅)₂(CN)(PPh₂C≡CPh)}] 6 and its precursor (NBu₄)[*cis*-Pt(C₆F₅)₂(CN)(PPh₂C≡CPh)] 3⁶² in acetonitrile ($\sim 4 \times 10^{-5}$ M; Supporting Information, Figure S4) are essentially identical, displaying only high absorptions at about 220 and 260 nm, respectively, assigned to ligand-centered transitions. However, in the solid state (Supporting Information, Figure S5) the presence in 6 of a low-energy absorption at 340 nm with a shoulder at 385 nm, which are absent in the precursor 3, is evidence of the Pt–Tl bond. Following previous assignments,^{24,31,34,82} these low energy absorptions are attributed to Pt(d_{z²) → Tl(6p_z) metal-to-metal charge transfer transitions (MM'CT). The absorption spectra in acetonitrile solution of 4 and 5 are similar (Supporting Information,}

(73) Janiak, C. *Coord. Chem. Rev.* **1997**, *163*, 107.

(74) Sawamura, M.; Iikura, H.; Nakamura, E. *J. Am. Chem. Soc.* **1996**, *118*, 12850.

(75) Hellmann, K. W.; Galka, C.; Gade, L. H.; Steiner, A.; Wright, D. S.; Kottke, T.; Stalke, D. *Chem. Commun.* **1998**, 549.

(76) Galka, C. H.; Gade, L. H. *Inorg. Chem.* **1999**, *38*, 1038.

(77) Gade, L. H. *Dalton Trans.* **2003**, 267.

(78) Hörner, M.; Manzoni de Oliveira, G.; Bresolin, L.; Bof de Oliveira, A. *Inorg. Chim. Acta* **2006**, *359*, 4631.

(79) Wiesbrock, F.; Schmidbaur, H. *J. Am. Chem. Soc.* **2003**, *125*, 3622.

(80) Sarazin, Y.; Hughes, D. L.; Kaltsoyannis, N.; Wright, J. A.; Bochmann, M. *J. Am. Chem. Soc.* **2007**, *129*, 881.

(81) Askarinejad, A.; Morsali, A. *J. Organomet. Chem.* **2006**, *691*, 3563.

(82) Ziegler, T.; Nagle, J. K.; Snijders, J. G.; Baerends, E. J. *J. Am. Chem. Soc.* **1989**, *111*, 5631.

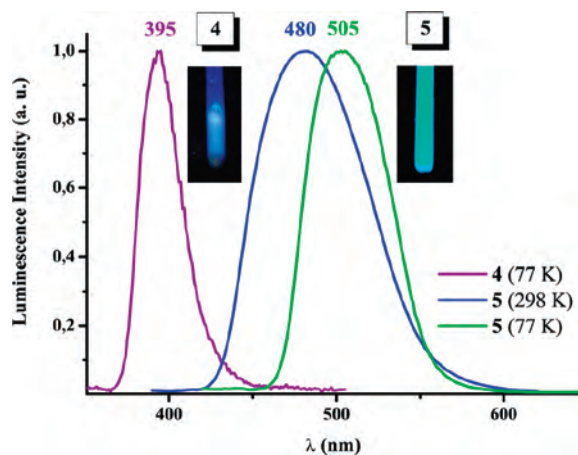


Figure 4. Normalized emission spectra of $[trans,trans,trans-Tl_2\{Pt(C_6F_5)_2(CN)_2\}]$ **4** in solid state (powder) at 77 K (λ_{exc} 340 nm) and of $[Tl\{Tl\{cis-Pt(C_6F_5)_2(CN)_2\}\}]$ **5** at room temperature (λ_{exc} 370 nm) and at 77 K (λ_{exc} 400 nm).

Figure S4) and differ from that of $(NBu_4)_2[trans-Pt(C_6F_5)_2(CN)_2]$ **1** (207, 220sh, 255, 265 nm) by the presence of a low-energy absorption feature (287 nm **4**, 285 nm **5**) that could be tentatively attributed to ligand-centered transitions perturbed by the presence of metals (Pt, Tl) in the monoanionic $[PtTl(C_6F_5)_2(CN)_2]^-$ fragments. As commented above (Scheme 2), this behavior is consistent with the partial rupture of Pt–Tl bonds in coordinative solvents such as acetone or acetonitrile. In the solid state, the white $[trans,trans,trans-Tl_2\{Pt(C_6F_5)_2(CN)_2\}]$ **4** differs from that of **1** (275 nm) in a band at 330 nm with a very small shoulder at 380 nm, which can be attributed to metal-centered $Pt(d_{z^2}) \rightarrow Tl(6p_z)$ charge transfer transitions of the Tl–Pt–Tl entity. The helical chain $\{Tl\{Tl\{cis-Pt(C_6F_5)_2(CN)_2\}\}\}$ **5** exhibits the low energy feature, remarkably red-shifted (ca. 400 nm), in accordance with its pale yellow color (Supporting Information, Figure S6). This low-energy band is also attributed to the formation of Pt–Tl bonds, and the remarkable red shift observed in **5** relative to **4** is obviously because of the presence of shorter Pt–Tl separations (3.0824(5) and 3.0997(5) Å in **5** vs 3.2087(3) Å in **4**).

All heteropolynuclear Pt–Tl complexes, except **4** at room temperature, show a bright emission when irradiated with UV–vis radiation, in contrast to the precursors **1** and **3**, which are not luminescent. This difference indicates that the emissions in **4–6** are probably a result of the interaction between the metal centers. In fact, the presence of Pt–Tl bonds has been often associated with luminescent properties^{23–35} although, however, several bi, trinuclear and also some extended systems containing Pt–Tl bonds have been found to be non emissive.^{36,39,40,50,53,57} At 77 K, complex $[trans,trans,trans-Tl_2\{Pt(C_6F_5)_2(CN)_2\}]$ **4** produces in solid state an intense luminescence with a maxima at 395 nm regardless of the excitation wavelength used (Figure 4). The excitation profile with three maxima at 310, 340, and 355 nm compares well to the absorption spectrum in the solid state (300, 330, and 380 nm) and is associated with the Tl–Pt–Tl chromophore. In solid state at room temperature, complex $\{Tl\{Tl\{cis-Pt(C_6F_5)_2(CN)_2\}\}\}$ **5** shows, independently of the excitation wavelength used, an intense blue–

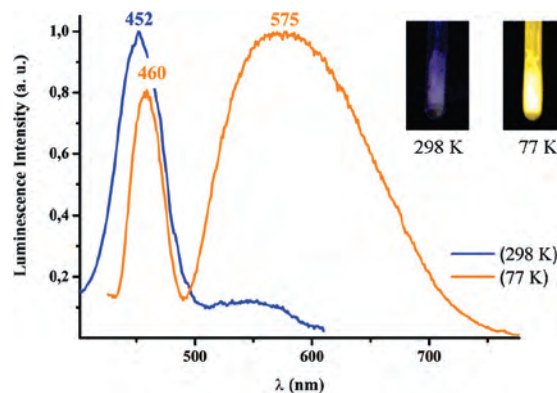


Figure 5. Normalized emission spectra of $[Tl\{cis-Pt(C_6F_5)_2(CN)(PPh_2C\equiv CPh)\}]$ **6** in solid state (powder) at room temperature (λ_{exc} 370 nm) and at 77 K (λ_{exc} 400 nm).

green luminescence at ~ 480 nm (excitation at 370 nm), which is slightly red-shifted at 77 K (~ 505 nm, excitation at 400 nm). The excitation spectra are also similar at both temperatures, showing a complicate profile from 300 to 420 nm. The red shift observed upon cooling (480 \rightarrow 505 nm) has been previously observed in other chain Pt–Tl systems, and it could be related to a decrease in the platinum–thallium separation caused by thermal contraction.^{23,24} The lifetime measurements determined by the phase-modulation technique in the solid state at room temperature display two components within the microsecond time scale $\tau_1 = 0.587 \mu s$ (61%) and $\tau_2 = 0.165 \mu s$ (39%), which indicate a phosphorescent nature of the emission. At room temperature, the white solid **6** exhibits a weak luminescence with two emission maxima at about 452 and 550 nm, respectively (Figure 5). Upon cooling at 77 K, the intensity of the emission is notably enhanced and both bands shift slightly to lower energies (460 and 575 nm). At 77 K, the excitation profile is slightly different depending on emission wavelength (peak maxima at 355, 400 nm λ_{em} 460 nm; 347, 370 nm λ_{em} 575 nm), which suggests the presence of different emissive states or centers in the solid. Lifetime measurements on both bands (7.3 μs , λ_{em}^{max} 460 nm; 13.7 μs , λ_{em}^{max} 575 nm) fit to a single exponential and are typical of phosphorescent processes. The behavior of this complex somewhat resembles that of the trinuclear complex $[PtTl_2(CN)_4]$.^{33,35} This compound presents at room temperature (300 K) an intense blue luminescence (448 nm, 0.25 μs), but at lower temperatures (≤ 77 K), a second red emission [457 nm (77 μs) and 577 nm (66 μs) at 1.4 K] appears.³³ The differences in the excitation spectra lead the authors to propose a model which involves different emissive triplet states associated with different centers for both bands.

The ground-state d^8-s^2 and $d^8-s^2-d^8$ bonding interactions and the emissive properties associated to it have been studied using different approaches.^{26,31,51,82,83} The remarkable overlap between the filled $5d_{z^2}$ orbitals of Pt and the empty $6p_z$ orbitals of thallium is responsible for the emissive behavior, which has been calculated (TDDFT) to have significant ($Pt 5d_{z^2} \rightarrow 6p_z$) charge transfer. According to these studies in

(83) Casado, M. A.; Pérez-Torrente, J. J.; López, J. A.; Ciriano, M. A.; Lahoz, F. J.; Oro, L. A. *Inorg. Chem.* **1999**, *38*, 2482.

[PtTl₂(CN)₄], the highest occupied molecular orbital possesses a mixed Pt–Tl–CN character and the lowest unoccupied molecular orbital is mainly Tl 6p_z in nature.⁵¹ It is worth noting that the emission energy for the helical chain in compound **5** is lower than for the expanded network **4** based on trinuclear “*trans,trans,trans*-Tl₂{Pt(C₆F₅)₂(CN)₂}²⁻” entities (Figure 4), a fact that has several precedents and that can be attributed to the expected lower band gap energy in the extended chain. In addition, the emission in **4** (395 nm) is remarkably blue-shifted in relation to complex **6**, a fact that is consistent with the longer Pt–Tl separation in **4** (3.2087(3) **4** vs 3.0756(3) Å in **6**).

Complexes **4–6** lose their emissive properties in solution at room temperature, probably because of total (**6**) or partial (**4, 5**) rupture of the Pt–Tl bonds. However, they show bright luminescence in frozen acetonitrile glasses (Supporting Information, Figures S7–S9). Not surprisingly, in **4** and **5** the color and the emissions are dependent on the solution concentration and excitation wavelength (Supporting Information, Figures S7, S8a–d). Thus, frozen (77 K) concentrated acetonitrile glasses of complex **4** (10⁻³ M–5 × 10⁻⁴ M), which are yellow in color, display two broad bands at ~530, 585 nm (λ_{exc} 350–450 nm), whose intensities and maxima are dependent on the excitation wavelengths (545, 605 nm, λ_{exc} 490, 10⁻³ M) (Supporting Information, Figure S7). Upon dilution (10⁻⁴ M–5 × 10⁻⁵ M, white), multiple emissions in the range 450–585 nm (10⁻⁴ M), 420–530 (5 × 10⁻⁵ M) are observed, depending on the excitation wavelength. At 2 × 10⁻⁵ M (white glasses) a band at 460 nm (λ_{exc} 330) with a shoulder at 520 (λ_{exc} 370 nm) is observed, and at 10⁻⁵ M the luminescence is lost. A similar behavior is observed for **5** (Supporting Information, Figure S8a–d). Frozen acetonitrile concentrated glasses (10⁻³ M) are yellow displaying broad low-energy bands (~500, 560–570 nm) and upon dilution (5 × 10⁻⁴ M–5 × 10⁻⁵ M, white), high energy emissions appear [420, 450, 480, 500, 550, 575 nm (5 × 10⁻⁴ M); 405, 460, 480, 550 nm (10⁻⁴ M–5 × 10⁻⁵ M)]. For all concentrations, the maxima are dependent on the excitation wavelength. In both complexes (**4** and **5**), as the concentration increases the intensity of the low-energy bands increases relative to those of the high-energy emissions. Accordingly, the PtTl interactions seem to be more favored in concentrated solutions. The behavior of complex **6** is somewhat different showing in frozen acetonitrile glasses (white for all concentrations used, 10⁻³ M–2 × 10⁻⁵ M), as in the solid state (77 K), two bands centered at 460 and ~560 nm, whose intensities depend on the concentration and the excitation wavelength (Supporting Information, Figure S9).

The frozen solution emission bands for the extended networks **4** and **5** are red-shifted beyond the solid state emission, specially favored in the most concentrated solutions. As has been previously noted in other d¹⁰ systems,^{24,25,84} the process of freezing the solution probably

causes the formation of different aggregates of the anionic fragments *trans* (**4**) or *cis* (**5**) [PtTl(C₆F₅)₂(CN)₂]_nⁿ⁻ or perhaps excimers or exciplexes with different degrees of Pt···Tl interactions in the various glasses. The fact that the excitation profiles are different depending on the concentration and wavelength emission used and the change of color observed in concentrated frozen solutions for **4** and **5** is suggestive of ground-state oligomerization. However, the variable-concentration luminescence study at 77 K for **6** indicates that in this complex the dimeric species observed in solid state could also exist in rigid glasses.

In summary, we have prepared the mixed *trans* and *cis* platinate complexes (NBu₄)₂[Pt(C₆F₅)₂(CN)₂] **1** and **2**, and examined their reactivity and that of related (NBu₄)[*cis*-Pt(C₆F₅)₂(CN)(PPh₂C≡CPh)] **3** toward Tl^I. It is interesting to note that while the [*trans*-Pt(C₆F₅)₂(CN)₂]²⁻ precursor bonds to two Tl⁺ centers (3.2087(3) Å) forming a typical pseudo-octahedron “Tl₂Pt(C₆F₅)₂(CN)₂”, which generates an extended two-dimensional layered structure [*trans,trans,trans*-Tl₂{Pt(C₆F₅)₂(CN)₂}·(CH₃COCH₃)₂]_n [**4**·(CH₃COCH₃)₂]_n by additional Tl^I···NC–Pt contacts, the [*cis*-Pt(C₆F₅)₂(CN)₂]²⁻ fragment only forms one direct Pt–Tl bond. In this case, an extended helical anionic [–Pt–Tl(1)–Pt–Tl(1)–]_nⁿ⁻ chain [**5**·(H₂O)]_n with two shorter Pt–Tl bonds (3.0824(5), 3.0997(5) Å) is generated. The second Tl^I center neutralizes the anionic chain through *intra* Tl^I···NC and Tl^I···o-F(C₆F₅) (*intra* and *inter*) electrostatic interactions. Neutralization of **3** yields a bimetallic “TlPt(C₆F₅)₂(CN)(PPh₂C≡CPh)” entity having a short Pt–Tl bond (3.0756(3) Å) and also stabilized by Tl^I···η(Ph), Tl^I···O(acetone), and Tl^I···o-F(*intra*) contacts. The existence of one additional secondary Tl^I···NC–Pt contact generates a discrete dimer [Tl{*cis*-Pt(C₆F₅)₂(CN)(PPh₂C≡CPh)}]₂ [**6**]₂. Spectroscopic data (NMR and UV) indicate that in complex **6**, the Pt–Tl bond is completely broken. However, for complex **4** and **5**, a partial dissociation takes place leading to a fast equilibrium, mainly between the corresponding monoanionic [PtTl(C₆F₅)₂(CN)₂]⁻ and dianionic [Pt(C₆F₅)₂(CN)₂]²⁻ fragments. In contrast to the precursors, which are not luminescent, all heteropolynuclear Pt–Tl complexes are emissive in solid state and in frozen acetonitrile solutions. The luminescence in solid state is attributed to Tl–Pt–Tl (**4,5**) or Pt–Tl (**6**) chromophores. However in frozen glasses the observed multiple emissions for **4** and **5** are likely due to aggregates based on anionic units [PtTl(C₆F₅)₂(CN)₂]_nⁿ⁻ with different degrees of Pt···Tl interactions.

Acknowledgment. This work was supported by the Spanish Ministerio de Educación y Ciencia (Project CTQ2005-08606-C02-01, 02 and a grant for A.G.).

Supporting Information Available: Experimental procedures, preparation, and characterization of **1** and **2**. Spectroscopic discussion for **1** and **2** and structural comments for **1**, Table S1 and Figures S1–S9 (PDF). Crystallographic data in CIF format. This material is available free of charge via the Internet at <http://pubs.acs.org>.

IC702180C

(84) Fernández, E. J.; Laguna, A.; López de Luzuriaga, J. M.; Monge, M.; Montiel, M.; Olmos, M. E. *Inorg. Chem.* **2007**, *46*, 2953.